

P-MapNet: Far-seeing Map Generator Enhanced by both SdMap and HdMap Priors

Zhou Jiang^{1,2*}, Zhenxin Zhu^{2,3*}, Pengfei Li^{2,4}, Huan-ang Gao^{2,4}, Tianyuan Yuan⁴, Yongliang Shi², Hang Zhao⁴, Hao Zhao^{2,†}

Abstract—Autonomous vehicles are gradually entering city roads today, with the help of high-definition maps (HdMaps). However, the reliance on HdMaps prevents autonomous vehicles from stepping into regions without this expensive digital infrastructure. This fact drives many researchers to study online HdMap generation algorithms, but the performance of these algorithms at far regions is still unsatisfying. We present P-MapNet, in which the letter P highlights the fact that we focus on incorporating map priors to improve model performance. Specifically, we exploit priors in both SdMap and HdMap. On one hand, we extract weakly aligned SdMap from OpenStreetMap, and encode it as an additional conditioning branch. Despite the misalignment challenge, our attention-based architecture adaptively attends to relevant SdMap skeletons and significantly improves performance. On the other hand, we exploit a masked autoencoder to capture the prior distribution of HdMap, which can serve as a refinement module to mitigate occlusions and artifacts. We benchmark on the nuScenes and Argoverse2 datasets. Through comprehensive experiments, we show that: (1) our SdMap prior can improve online map generation performance, using both rasterized (by up to +18.73 mIoU) and vectorized (by up to +8.50 mAP) output representations. (2) our HdMap prior can improve map perceptual metrics by up to 6.34%. (3) P-MapNet can be switched into different inference modes that covers different regions of the accuracy-efficiency trade-off landscape. (4) P-MapNet is a far-seeing solution that brings larger improvements on longer ranges. Codes and models are publicly available at <https://jike5.github.io/P-MapNet/>.

I. INTRODUCTION

While we still don't know the ultimate answer to fully autonomous vehicles that can run smoothly in each and every corner of the earth, the community does have seen some impressive milestones, e.g., robotaxis are under steady operation in some big cities now. Yet current autonomous driving stacks heavily depend on an expensive digital infrastructure: HdMaps. With the availability of HdMaps, local maneuvers are reduced to lane following and lane changing coupled with dynamic obstacle avoidance, significantly narrowing down the space of decision making. But the generation of HdMaps, which is shown in the left-top panel of Fig. 1, is very cumbersome and expensive. And what's worse, HdMaps cannot be generated for good and all, because they must be updated every three months on average. It is widely recognized that reducing reliance on HdMaps is critical.

*Equal contribution, †Corresponding author

¹Beijing Institute of Technology, China, jzian@bit.edu.cn.

²Institute for AI Industry Research (AIR), Tsinghua University, China, zhaohao@air.tsinghua.edu.cn.

³Beihang University, China, zhuzhenxin@buaa.edu.cn.

⁴Tsinghua University, China.

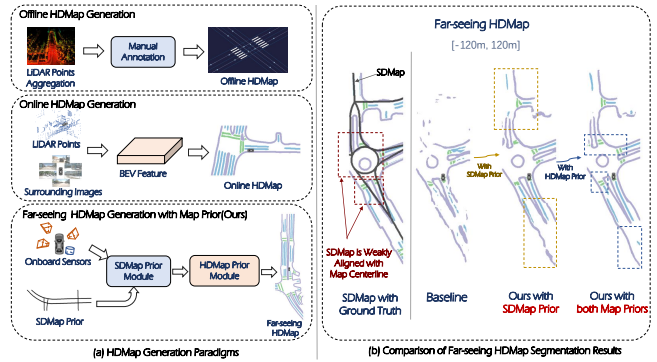


Fig. 1. Left: Since offline HdMap generation is cumbersome and expensive, people are pursuing online HdMap generation algorithms and our P-MapNet is an online HdMap generator enhanced by both SdMap and HdMap priors. Right: Despite the misalignment between SdMaps and HdMaps, our P-MapNet can significantly improve map generation performance, especially on the far side.

Thus, several recent methods [14], [17] generate HdMaps using multi-modal online sensory inputs like LiDAR point clouds and panoramic multi-view RGB images, and a conceptual illustration of this paradigm is given in the left-middle panel of Fig. 1. Despite promising results achieved by these methods, long range distance online HdMap generators still report limited quantitative metrics and this study focuses on promoting their performance using priors. Specifically, two sources of priors are exploited: SdMap and HdMap, as demonstrated in the left-bottom panel of Fig. 1.

SdMap Prior. Before the industry turns to build the digital infrastructure of HdMaps on a large scale, Standard Definition Maps (SdMaps) have been used for years and have largely promoted the convenience of our daily lives. Commercial SdMap applications provided by Google or Baidu help people navigate big cities with complex road networks, telling us to make turns at crossings or merge into main roads. SdMaps are not readily useful for autonomous cars because they only provide center-line skeletons (noted as SdMap Prior in the left-bottom panel of Fig. 1). So we aim to exploit SdMap priors to build better online HdMap generation algorithms, which can be intuitively interpreted as *drawing* Hdmaps around the skeleton of SdMaps. However, this intuitive idea faces a primary challenge: misalignment. Per implementation, we extract SdMaps from OpenStreetMap using GPS signals but unfortunately they are, at best, weakly aligned with the ground truth HdMap in a certain scenario. An illustration is given in the right panel of Fig. 1, noted as SdMap with Ground Truth. To this end, we leverage an

attention based network architecture that adaptively attends to relevant SDMap features and successfully improve the performance by large margins in various settings (see Table. I).

HDMap Prior. Although useful, SDMap priors cannot fully capture the distribution of HDMap output space. As noted by Ours with SDMap Prior in the right panel of Fig. 1, HDMap generation results are broken and unnecessarily curved. This is credited to the fact that our architecture is, like prior methods, designed in a BEV dense prediction manner and the structured output space of BEV HDMap cannot be guaranteed. As such, HDMap prior comes to the stage as a solution and the intuition is that if the algorithm models the structured output space of HDMaps explicitly, it can naturally correct these unnatural artifacts (i.e., broken and unnecessarily curved results mentioned above). On the implementation side, we train a masked autoencoder (MAE) on a large set of HDMaps to capture the HDMap prior and use it as a refinement module. As noted by ours with both Map Priors in the right panel of Fig. 1, our MAE successfully corrects aforementioned issues.

P-MapNet as a far-seeing solution. A closer look at the positive margins brought by incorporating priors reveals that P-MapNet is a far-seeing solution. As shown in the right panel of Fig. 1, after incorporating the SDMap prior, missing map elements far from the ego vehicle (denoted by the car icon) are successfully extracted. This is understandable as the road center-line skeletons on the far side are already known in the SDMap input. Meanwhile, the HDMap prior brings improvements in two kinds of regions: crossings with highly structured repetitive patterns and lanes on the far side. This is credited to the fact that our masked autoencoder can incorporate the priors about how typical HDMaps look like, e.g., lanes should be connected and largely straight and crossings are drawn in a repetitive manner. As Table. I demonstrates, positive margins steadily grow along with the sensing range. We believe P-MapNet, as a far-seeing solution, is potentially helpful in deriving more intelligent decisions that are informed of maps on the far side.

In summary, our contributions are three-fold: (1) We incorporate SDMap priors into online map generators by attending to weakly aligned SDMap features and achieve significant performance improvements; (2) We also incorporate HDMap priors using a masked autoencoder as a refinement module, correcting artefacts that deviate the structured output space of HDMaps; (3) We achieve state-of-the-art results of *far-seeing* HDMap generation on public benchmarks and present in-depth ablative analyses revealing the mechanism.

II. RELATED WORK

A. Online HD Map generation

Online map generators are important for autonomous driving [12] [23] [32] [25] [13], which is similar in spirit to room layout estimation [31] [3] [7] for indoor scenes. Traditionally, HD maps are manually annotated offline, combining point cloud maps via SLAM algorithms [1], [11] for high accuracy but at a high cost and without real-time updates. In contrast, recent efforts have focused on utilizing onboard sensors

for the efficient and cost-effective generation of online HD maps [5], [14], [15], [17], [20], [21]. HDMapNet [14] employs pixel-wise labelling and heuristic post-processing, using Average Precision (AP) and Intersection over Union (IoU) as metrics. More recent approaches [4], [16], [17], [28], [29], have adopted end-to-end vectorized HD map generation techniques, leveraging Transformer architectures [22]. However, these methods rely solely on onboard sensors and have limitations in handling challenging environmental conditions like occlusions or adverse weather.

B. Long-range Map Perception

To enhance the practicality of HD maps for downstream tasks, some studies aim to extend their coverage to longer perception ranges. SuperFusion [5] combines LiDAR point clouds and camera images for depth-aware BEV transformation, yielding forward-view HD map predictions up to 90 *m*. NeuralMapPrior [27] maintains and updates a global neural map prior, enhancing online observations to generate higher-quality, extended-range HD map predictions. [8] proposes using satellite maps to aid online map generation. Features from onboard sensors and satellite images are aggregated through a hierarchical fusion module to obtain the final BEV features. MV-Map [26] specializes in offline, long-range HD map generation. It aggregates all relevant frames during traversal and optimizes neural radiance fields for improved BEV feature generation.

III. FORMULATION

Given the LiDAR point cloud \mathcal{P} and panoramic images $\{\mathcal{I}_i \mid i = 1, 2, \dots, N\}$, where N is typically six for a panoramic rig, a common online HDMap generation task (e.g., HDMapNet [14]) can be formulated as:

$$\mathcal{M} = \mathcal{F}_2(\mathcal{F}_1(\mathcal{P}, \mathcal{I})), \quad (1)$$

where \mathcal{F}_1 represents the feature extractor that takes multi-modal inputs and generates BEV features, while \mathcal{F}_2 is a segmentation head that predicts a semantic category label for each grid in the BEV. And \mathcal{M} is the HDMap prediction.

However, this common formulation fails to leverage the rich priors in SDMap and HDMap. So we formulate a new task to incorporate these priors to produce a more accurate and *far-seeing* HDMap, thereby effectively addressing issues pertaining to occlusion as well as super long range sensing:

$$\mathcal{M}' = \mathcal{H}(\mathcal{F}_2(\mathcal{F}_1(\mathcal{P}, \mathcal{I}, \mathcal{S}))), \quad (2)$$

Here \mathcal{S} is the SDMap prior that comes in the form of road center-line skeletons. \mathcal{H} represents the refinement module which is a pre-trained model capturing the distribution characteristics of HDMap. Similarly, \mathcal{M}' is the *far-seeing* HDMap prediction over 100 meters on the front/back side.

Output Format. There are two typical output formats for online HDMap generation: rasterized and vectorized. In this study, we focus on the rasterized representation (e.g. HDMapNet [14]), as it is more suitable for designing our

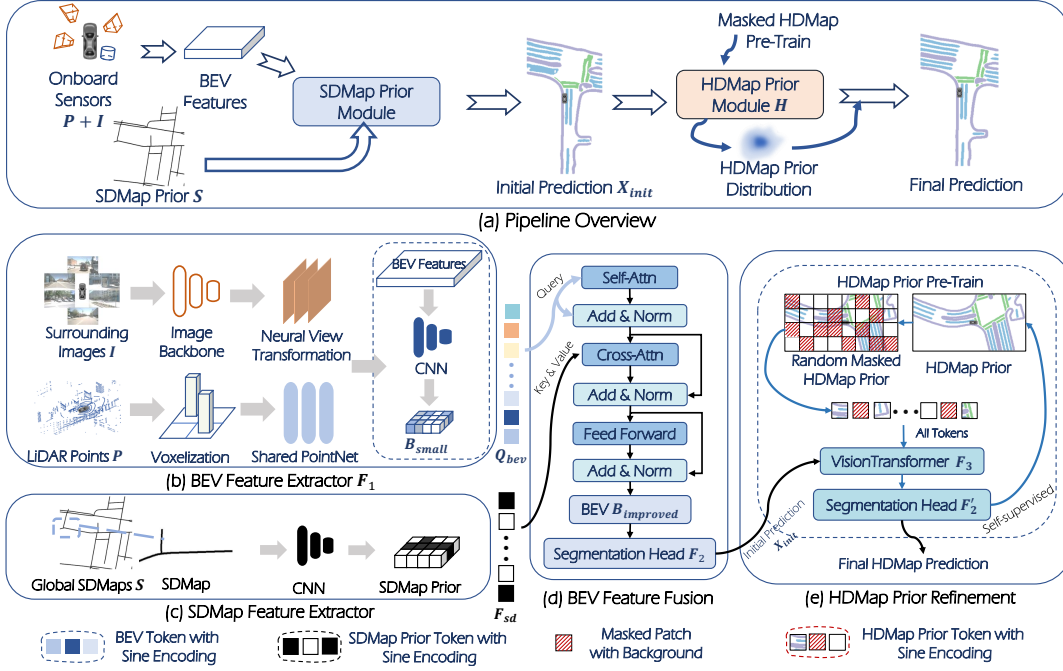


Fig. 2. **P-MapNet overview.** P-MapNet is designed to accept either surrounding cameras or multi-modal inputs. It processes these inputs to extract sensors features and SDMap priors features, both represented in the Bird’s Eye View (BEV) space. These features are then fused using an attention mechanism and subsequently refined by the HDMap prior module to produce results that closely align with real-world map data.

two prior modules (than vectorized counterpart). Specifically, how to effective encode vectorized representation for input/output is not as natural as rasterized representation.

S-only setting. Shown in Fig. 2(a), we incorporate SDMap prior by encoding center-line skeletons as an additional input branch. In this \mathcal{S} -only setting, the formulation is:

$$\mathcal{M}_S = \mathcal{F}_2(\mathcal{F}_1(\mathcal{P}, \mathcal{I}, \mathcal{S})), \quad (3)$$

where the procedure of encoding \mathcal{S} is illustrated in Fig. 2(c).

S+H setting. While the SDMap prior \mathcal{S} is naturally incorporated as an additional input, leveraging the HDMap prior is challenging. Our innovative proposal is to incorporate HDMap prior using a masked auto-encoder (MAE) as a refinement module. The core idea is to use MAE for the reconstruction of HDMaps so that this MAE intrinsically capture the distribution of HDMap prior. However, this is not trivial as the vanilla MAE cannot achieve this goal.

Vanilla MAE. A vanilla MAE [10] would treat HDMaps as images and trains under an MSE loss for image reconstruction. The problem is that this MAE would predict images thus cannot be used as a refinement module, as our HDMap generator actually needs a segmentation head at last.

Our MAE variant. Our MAE variant takes rasterized HDMap (which is in nature images) as input, but predicts the semantic label of each grid using a segmentation head. This is still an auto-encoding process since the module reconstructs the HDMap of interest. However, this MAE’s input and output comes in different formats: images and segmentation masks. This readily allows refinement when attached after the \mathcal{M}_S output mentioned above.

Formal notation. our HDMap refinement module has two

training steps. The first step is to pre-train the HDMap Prior Module on a large set of HDMaps, as shown in Fig. 2(e).

$$\begin{aligned} \mathcal{M}_{\text{self}} &= \mathcal{H}(\mathcal{M}_{\text{masked}}) \\ &\triangleq \mathcal{F}'_2(\mathcal{F}_3(\mathcal{M}_{\text{masked}})), \end{aligned} \quad (4)$$

Here the HDMap Prior Module $\mathcal{H}(\cdot)$ is specifically defined as $\mathcal{F}'_2(\mathcal{F}_3(\cdot))$, of which \mathcal{F}_3 denotes a ViT model used in typical MAEs. But \mathcal{F}'_2 denotes another segmentation head, as mentioned above. This \mathcal{F}'_2 makes our MAE a variant ready for refinement. $\mathcal{M}_{\text{masked}}$ is the randomly masked HDMap from the training dataset and $\mathcal{M}_{\text{self}}$ is the unmasked version.

Fine-tuning. The second step is end-to-end fine-tuning:

$$\begin{aligned} \mathcal{M}' &= \mathcal{H}(\mathcal{M}_S) \\ &\triangleq \mathcal{F}'_2(\mathcal{F}_3(\mathcal{M}_S)), \end{aligned} \quad (5)$$

where \mathcal{M}_S is the initial prediction from SDMap Prior Module, as depicted in Fig. 2(a) and Equation.3.

As such, the formal $\mathcal{S}+\mathcal{H}$ setting (by integrating Equation.3 and Equation.5) is shown as:

$$\mathcal{M}' = \mathcal{F}'_2(\mathcal{F}_3(\mathcal{F}_2(\mathcal{F}_1(\mathcal{P}, \mathcal{I}, \mathcal{S})))) \quad (6)$$

IV. METHOD

A. SDMap Prior Module

Now we elaborate on the implementation of our SDMap prior module, and first we recap the motivation again: Given the intrinsic challenges associated with onboard sensing, such as distant road invisibility and adverse weather conditions, incorporating SDMap prior becomes a promising technique, as SDMap provides a stable and consistent outlining of the environment (agnostic of those challenges).

SDMap Generation. We first introduce our approach to generate SDMap priors by leveraging OpenStreetMap (OSM) [9] data. We specifically employ the nuScenes [2] and Argoverse2 [24] datasets for our research, as these datasets hold a prominent position within the autonomous driving domain. These datasets are richly equipped with sensors but do not include the corresponding SDMap information for the captured regions. To address this limitation, we leverage OpenStreetMap to obtain the relevant SDMap data for these regions. Specifically, we first obtain the localized SDMap data of the corresponding area from the OSM¹ based on the on-board GPS information. Then these SDMap data are transformed to the ego vehicle’s coordinate system. Although we obtain the SDMap priors, the problem of misalignment due to the low accuracy of the OSM and the bias of the GPS will pose a challenge to the fusion of SDMap priors.

Incorporating SDMap Prior. After extraction and rasterization, the rasterized SDMap prior inevitably faces spatial misalignment, where the SDMap prior doesn’t align precisely with the current operational location, often resulting from inaccurate GPS signals or rapid vehicle movement. This misalignment renders the straightforward method of directly concatenating BEV features with SDMap features in the feature dimension ineffective, as detailed in Tab.VI. To tackle this challenge, we adopt a multi-head cross-attention module. This allows the network to utilize cross-attention to determine the most suitably aligned location, thereby effectively enhancing the BEV feature with the SDMap prior.

BEV Query. As illustrated in Fig. 2(b), we first utilize a convolutional network to downsample the BEV features. This not only averts excessive memory consumption on low-level feature maps but also partially alleviates the misalignment between the image BEV features and the LiDAR BEV features. The downsampled BEV features are represented as $\mathcal{B}_{\text{small}} \in \mathbb{R}^{\frac{H}{d} \times \frac{W}{d} \times C}$, where d is the downsampling factor. These features, combined with sine positional embedding and squeezed into 1D, resulting in the BEV queries \mathcal{Q}_{bev} .

SDMaps Prior attended. The associated (though misaligned) SDMap undergoes processing via a convolutional network in conjunction with sine positional embedding, producing the SDMap prior tokens \mathcal{F}_{sd} , as shown in Fig. 2(c). Subsequently, the multi-head cross-attention is employed to enhance the BEV queries by integrating the information from SDMap priors. The formal representation is,

$$\begin{aligned} \mathcal{Q}' &= \text{Concat}(\text{CA}_1(\mathcal{Q}_{\text{bev}}, \mathcal{F}_{\text{sd}}), \dots, \text{CA}_m(\mathcal{Q}_{\text{bev}}, \mathcal{F}_{\text{sd}})), \\ \mathcal{B}_{\text{improved}} &= \text{layernorm}(\mathcal{Q}_{\text{bev}} + \text{Dropout}(\text{Proj}(\mathcal{Q}'))), \end{aligned} \quad (7)$$

where the CA_i is the i -th single head cross-attention, m is the number of head, key and value embeddings, Proj is a projection layer and $\mathcal{B}_{\text{improved}}$ represents the resized BEV feature derived from the multi-head cross-attention that incorporates the SDMap prior. Subsequently, the improved BEV features pass through a segmentation head to get the initial HDMap element prediction, denoted as $X_{\text{init}} \in \mathbb{R}^{H \times W \times (N_c+1)}$. Here,

the (N_c+1) channels denote the total number of map element classes, including an additional background class.

B. HDMap Prior Module

Then we describe the HDMap prior module, which \mathcal{H} is computationally heavy (see Fig.5) which is indeed optional. Our goal is to acquire a more precise and realistic *far-seeing* HDMap, particularly in challenging scenarios such as inclement weather, areas of occlusion, and regions of invisibility. To enhance the continuity and realism of HDMap generation in these scenarios, closely approximating the distribution of HDMap, we employ an adapted pre-trained MAE module to capture the distribution. Training the HDMap Prior Module has two training steps: the first step involves training the MAE module using self-supervised learning to capture the HDMap distribution and the second step is fine-tuning by loading weights in the first step and using the initial HDMap prediction X_{init} as input, as shown in Function. 5.

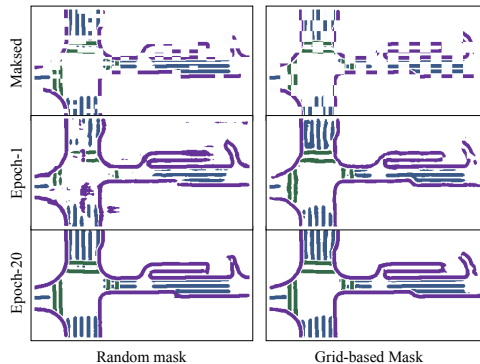
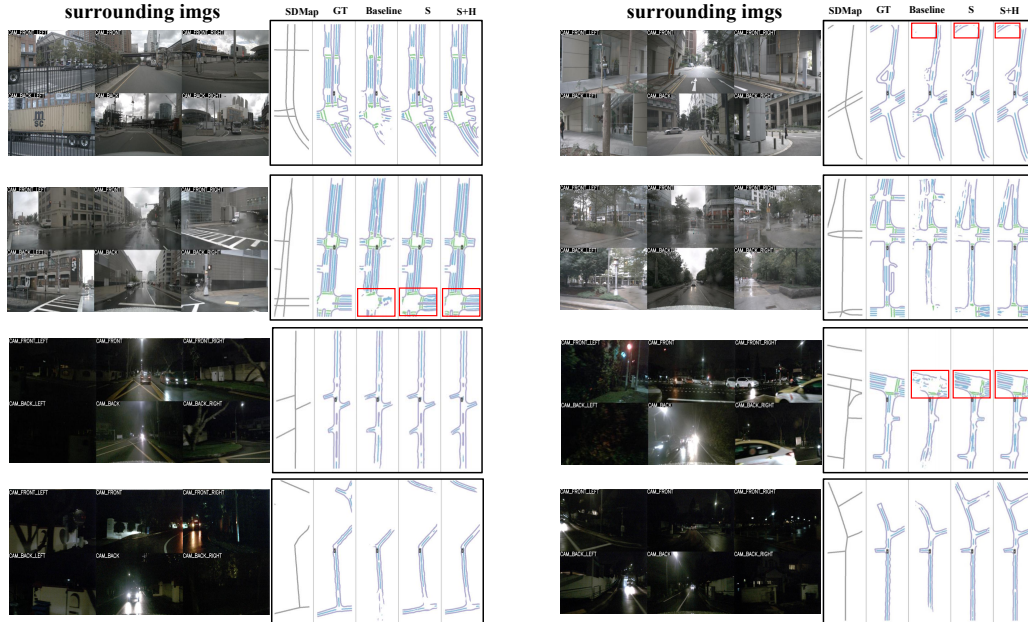


Fig. 3. **Different mask strategies.** “Masked” refers to the pre-training inputs after applying various masking strategies, and “Epoch-1” and “Epoch-20” denote the reconstruction results at the first and twentieth epochs of the pre-training process, respectively.

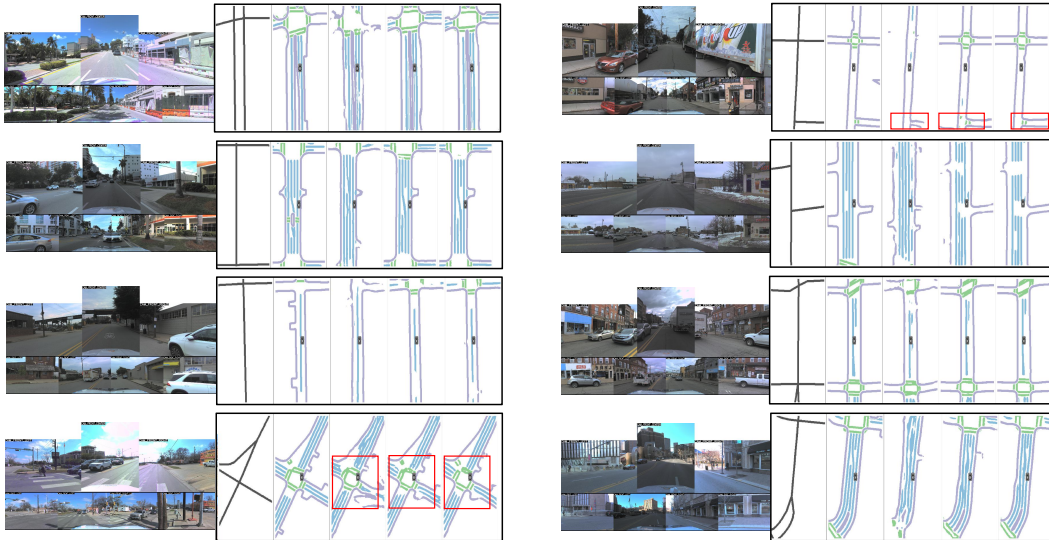
Pre-trained MAE module. We utilize self-supervised learning to pre-train the masked autoencoder to capture the data distribution of HDMap. As shown in Fig. 2(e), this module consists of a Vision Transformer model [6] and a fully convolutional segmentation head. As illustrated in Function. 4, we mask the HDMap ground truth in the *training* set of the dataset, and then encode this masked HDMap using the ViT model. Subsequently, given that our reconstruction target is indeed a semantic mask (although treated as images for input), we employ the segmentation head to revert the masked HDMap back to its original HDMap ground truth. This process is self-supervised using pixel-wise cross-entropy loss between the HDMap ground truth and the masked HDMap. Specifically, we tried two different mask strategy to pre-train the module, namely grid mask and random mask, as shown in Fig. 9. In the random mask strategy, we randomly select both the mask patch size and the mask ratio from a set of candidates to mitigate the over-fitting issue during pre-training.

End-to-end fine-tuning. Next we apply the pre-trained MAE module on the initial HDMap prediction X_{init} as a refinement plug-in to improve the initially predicted HDMap,

¹<https://www.openstreetmap.org/>



(a) Qualitative Results on nuScenes within the range of 240m*60m.



(b) Qualitative Results on Argoverse2 within the range of 120m*60m.

Fig. 4. **Qualitative results.** We conduct a comparative analysis within a range of $240m \times 60m$ on nuScenes dataset and $120m \times 60m$ on Argoverse2 dataset, utilizing C+L as input. In our notation, “S” indicates that our method utilizes only the SDMap priors, while “S+H” indicates the utilization of both. Our method consistently outperforms the baseline method under various weather conditions and in scenarios involving viewpoint occlusion.

addressing potential issues such as broken or missing lanes in challenging scenarios. We then take the entire model through some lightweight fine-tuning for 10 epochs to better align the distribution of the initial prediction with that of the HDMap distribution, as illustrated in Function 5.

V. EXPERIMENTS

A. Dataset and Metrics

We evaluate P-MapNet on two popular datasets in autonomous driving research, nuScenes [2] and Argoverse2 [24]. To demonstrate our method is a far-seeing solution, we set three distinct perception ranges along the direction of vehicle travel: $60 \times 30m$, $120 \times 60m$, $240 \times 60m$.

Additionally, we utilize different map resolutions, specifically $0.15m$ for the short range of $60 \times 30m$ and $0.3m$ for the rest two longer ranges. We use intersection-over-union (IoU) as the metrics for segmentation results and incorporate a post-processing step to get the vectorized map and evaluate it using the average precision (AP). Following [5], we set the threshold of IoU as 0.2 and threshold of CD as 0.5m, 1.0m, 1.5m. Furthermore, to evaluate the *realism* of the HDMap prior refinement module output, we utilize a perceptual metric LPIPS [30], which leverages deep learning techniques to more closely simulate human visual perception differences, providing a more precise and human vision-aligned image quality assessment than traditional pixel-level

TABLE I

QUANTITATIVE RESULTS OF IOU SCORES AND AP SCORES. PERFORMANCE COMPARISON OF HDMAPNET [14] BASELINE AND OURS ON THE NUSCENES VAL SET [2]. ‘‘S’’ INDICATES THAT OUR METHOD UTILIZES ONLY THE SDMAP PRIORS, WHILE ‘‘S+H’’ INDICATES THE UTILIZATION OF THE BOTH PRIORS. ‘‘M’’ REPRESENTS THE MODALITY OF OUR METHOD AND ‘‘EPOCH’’ REPRESENTS THE NUMBER OF REFINEMENT EPOCHS.

Range	Method	S	S+H	M	Epoch	Div.	Ped.	Bound.	mIoU	Div.	Ped.	Bound.	mAP	FPS
60 × 30 m	HMapNet			C	30	40.5	19.7	40.5	33.57	27.68	10.26	45.19	27.71	35.4
	P-MapNet	✓		C	30	44.1	22.6	43.8	36.83 (+3.26)	32.11	11.33	48.67	30.70 (+2.99)	30.2
	P-MapNet	✓	✓	C	10	44.3	23.3	43.8	37.13 (+3.56)	26.08	17.66	48.43	30.72 (+3.01)	12.2
	HMapNet			C+L	30	45.9	30.5	56.8	44.40	29.46	13.89	54.07	32.47	21.4
	P-MapNet	✓		C+L	30	53.3	39.4	63.1	51.93 (+7.53)	36.56	20.06	60.31	38.98 (+6.51)	19.2
	P-MapNet	✓	✓	C+L	10	54.2	41.3	63.7	53.07 (+8.67)	37.81	24.96	60.90	41.22 (+8.75)	9.6
120 × 60 m	HMapNet			C	30	39.2	23.0	39.1	33.77	14.40	8.98	34.99	19.46	34.2
	P-MapNet	✓		C	30	44.8	30.6	45.6	40.33 (+6.56)	19.39	14.59	38.69	24.22 (+4.76)	28.7
	P-MapNet	✓	✓	C	10	45.5	30.9	46.2	40.87 (+7.10)	19.50	24.72	42.48	28.90 (+9.44)	12.1
	HMapNet			C+L	30	53.6	37.8	57.1	49.50	21.11	18.90	47.31	29.11	21.2
	P-MapNet	✓		C+L	30	63.6	50.2	66.8	60.20 (+10.70)	28.30	25.67	52.51	35.49 (+6.38)	18.7
	P-MapNet	✓	✓	C+L	10	65.3	52.0	68.0	61.77 (+12.27)	30.63	28.42	53.27	37.44 (+8.33)	9.6
240 × 60 m	HMapNet			C	30	31.9	17.0	31.4	26.77	7.37	5.09	21.59	11.35	22.3
	P-MapNet	✓		C	30	46.3	35.7	44.6	42.20 (+15.43)	10.86	12.74	25.52	16.38 (+5.03)	19.2
	P-MapNet	✓	✓	C	10	49.0	40.9	46.6	45.50 (+18.73)	14.51	25.63	28.11	22.75 (+11.40)	9.1
	HMapNet			C+L	30	40.0	26.8	42.6	36.47	11.29	11.40	29.05	17.25	13.1
	P-MapNet	✓		C+L	30	52.0	41.0	53.6	48.87 (+12.40)	17.87	20.00	35.89	24.59 (+7.34)	10.9
	P-MapNet	✓	✓	C+L	10	53.0	42.6	54.2	49.93 (+13.46)	21.47	24.14	34.23	26.61 (+9.36)	6.6

TABLE II

P-MAPNET ACHIEVES STATE-OF-THE-ART ON NUSCENES val SET.

THE SYMBOL ‘‘†’’ DENOTES RESULTS REPORTED IN [26], [5], WHILE ‘‘NMP’’ REPRESENTS THE ‘‘HDMAPNET+NMP’’ CONFIGURATION AS DESCRIBED IN [27]. FOR SUPERLONG-RANGE PERCEPTION, WE COMPARED WITH SUPERFUSION [5] AND BEVFUSION [18]. ‘‘C’’ AND ‘‘L’’ RESPECTIVELY REFER TO THE SURROUND-VIEW CAMERAS AND LIDAR INPUTS. OURS USES BOTH SDMAP AND HDMAP PRIORS.

Range	Method	Modality	Div.	Ped.	Bound.	mIoU
60 × 30 m	VPN [19] †	C	36.5	15.8	35.6	29.30
	Lift-Splat-Shoot [20] †	C	38.3	14.9	39.3	30.83
	HMapNet [14]	C	40.5	19.7	40.5	33.57
	NMP [27] †	C	44.1	21.0	46.1	37.05
	HMapNet	C+L	45.9	30.5	56.8	44.40
	P-MapNet (Ours)	C	44.3	23.3	43.8	37.13
P-MapNet (Ours)	C+L	54.2	41.3	63.7	53.07	
90 × 30 m	BEVFusion [18] †	C+L	33.9	18.8	38.8	30.50
	SuperFusion [5] †	C+L	37.0	24.8	41.5	34.43
	P-MapNet (Ours)	C+L	44.73	31.03	45.5	40.64

or simple structural comparisons. Implementation details can be found in the supplementary material.

B. Results

Comparisons with State-of-the-arts. We conducted a comparative analysis of our approach with current state-of-the-art (SOTA) approaches in both short-range (60m × 30m) perception and long-range (90m × 30m) with a resolution of 0.15m. As indicated in Tab. II, our method exhibits superior performance compared to both existing vision-only and multi-modal (RGB+LIDAR) methods.

Far-seeing Experiments. We performed a performance comparison with HMapNet [14] at various distances and using different sensor modalities, with the results summarized in Tab. I and Tab. III. Our method achieves a remarkable 13.4% improvement in mIOU at a range of 240m × 60m. It is noteworthy that the effectiveness of SD Map priors becomes more pronounced as the perception distance extends beyond or even surpasses the sensor detection range, thus validating the efficacy of SD Map priors. Lastly, our utiliza-

tion of HD Map priors contributes to additional performance improvements by refining the initial prediction results to be more realistic and eliminating results that are broken and unnecessarily curved, as demonstrated in Fig. 4.

TABLE III

QUANTITATIVE RESULTS OF MAP SEGMENTATION ON ARGOVERSE2 val SET. WE CONDUCTED A COMPARISON BETWEEN THE P-MAPNET METHOD AND HDMAPNET [14], USING ONLY SURROUND-VIEW CAMERAS AS INPUT, DEMONSTRATING SUPERIOR PERFORMANCE.

Range	Method	Div.	Ped.	Bound.	mIoU
60 × 30 m	HMapNet	53.0	27.9	44.5	41.80
	P-MapNet (S)	52.9	29.7	46.8	43.13 (+1.33)
	P-MapNet (S+H)	53.5	30.1	47.3	43.63 (+1.83)
120 × 60 m	HMapNet	48.3	27.8	40.0	38.70
	P-MapNet (S)	52.5	34.3	48.7	45.17 (+6.47)
	P-MapNet (S+H)	53.1	34.7	49.0	45.60 (+6.90)

Perceptual Metric of HDmap Prior. The HMap Priors Module endeavors to map the network output onto the distribution of HDMaps to make it more *realistic*. To evaluate the *realism* of the HMap prior refinement Module output, we utilize a perceptual metric LPIPS [30] (lower values indicate better performance). The enhancements achieved in the S+H setting are considerably greater when compared to those in the S-only setting as demonstrated in Tab.IV.

Vectorization Results. We also conducted a comparison of vectorization results by employing post-processing to obtain vectorized HD Maps. As detailed in Tab. I, we achieve the best instance detection AP results across distance ranges.

Does SDMap prior work for direct vectorized map prediction? As demonstrated in Tab.IX, to confirm the universality of our SDMap prior, we integrated our SDMap Prior Module into MapTR [16] (with only minor modifications), an end-to-end framework, referred to as the MapTR-SDMap method. Our MapTR-SDMap method also led to a significant improvement in mean Average Precision (mAP).

TABLE IV

PERCEPTUAL METRIC OF HDMAP PRIOR. WE UTILIZE THE LPIPS METRIC TO EVALUATE THE *realism* OF S+H MODELS ON $120m \times 60m$ PERCEPTION RANGE. AND THE IMPROVEMENTS IN THE S+H SETTING ARE MORE SIGNIFICANT COMPARED TO THOSE IN THE S-ONLY SETTING.

Range	Method	Modality	mIoU \uparrow	LPIPS \downarrow	Modality	mIoU \uparrow	LPIPS \downarrow
$120 \times 60 m$	Baseline	C	33.77	0.8050	C+L	49.07	0.7872
	P-MapNet (S)	C	40.33 (+6.56)	0.7926 (1.54%)	C+L	60.20 (+11.13)	0.7607 (3.37%)
	P-MapNet (S+H)	C	40.87 (+7.10)	0.7717 (4.14%)	C+L	61.77 (+12.70)	0.7124 (9.50%)
$240 \times 60 m$	Baseline	C	26.77	0.8484	C+L	36.47	0.8408
	P-MapNet (S)	C	42.20 (+15.43)	0.8192 (3.44%)	C+L	48.87 (+12.40)	0.8097 (3.70%)
	P-MapNet (S+H)	C	45.50 (+18.73)	0.7906 (6.81%)	C+L	49.93 (+13.46)	0.7765 (7.65%)

TABLE V

COMPARISONS WITH MAPTR [16] ON NUSCENES *val* SET. WE CONDUCTED A COMPARISON BETWEEN MAPTR FUSED WITH THE SDMAP PRIOR METHOD (MAPTR-SDMAP) AND THE VANILLA MAPTR [16], USING ONLY SURROUND-VIEW CAMERAS AS INPUT AND WE USE PREDEFINED CD THRESHOLDS OF 0.5M, 1.0M AND 1.5M. OUR RESULTS DEMONSTRATED SUPERIOR PERFORMANCE, HIGHLIGHTING THE EFFECTIVENESS OF OUR SDMAP PRIOR FUSION METHOD.

Range	Method	Div.	Ped.	Bound.	mAP
$60 \times 30 m$	MapTR [16]	49.50	41.17	51.08	47.25
	MapTR-SDMap	50.92	43.71	53.49	49.37 (+2.21)
	P-MapNet	26.08	17.66	48.43	30.72
$120 \times 60 m$	MapTR [16]	26.00	18.89	15.73	20.20
	MapTR-SDMap	27.23	21.95	19.50	22.89 (+2.69)
	P-MapNet	19.50	24.72	42.48	28.90
$240 \times 60 m$	MapTR [16]	12.69	7.17	4.23	8.03
	MapTR-SDMap	22.74	16.34	10.53	16.53 (+8.50)
	P-MapNet	14.51	25.63	28.11	22.75

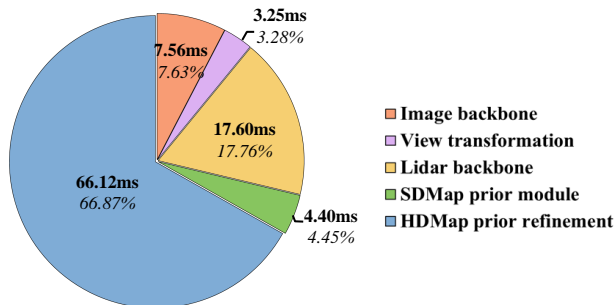


Fig. 5. **Detailed runtime.** We conduct runtime profiling of each component in P-MapNet at a range of $60 \times 120m$ on one RTX 3090 GPU.

C. Ablation Study

All ablative experiments are conducted on nuScenes val set with a perception range of $120m \times 60m$ and the camera-LiDAR fusion(C+L) configuration.

Detailed Runtime. In Fig. 5, we provide the detailed wallclock runtime of each component in P-MapNet with both camera and LiDAR inputs. As a recap, a complete FPS evaluation is reported in Tab. I. As shown by the profiling, the HDMap prior is computationally heavy but it is indeed optional. Practitioners can switch between the SDmap only setting or the SDMap+HDMap setting, depending on the computation overhead (e.g., onboard or offboard).

SDMap Prior Fusion Strategies. To validate the effectiveness of our proposed fusion approach for SDMap priors, we experimented with various fusion strategies, the details of which are summarized in Tab. VI. In an initial evaluation, a

TABLE VI

ABLATIONS ABOUT SD MAPS FUSION STRATEGIES. THE EXPERIMENTS ARE CONDUCTED WITH RANGE OF $120 \times 60m$ AND C+L AS INPUTS. “W/O SDMAP” IS THE BASELINE [14]. “W/O SDMAP, W SELF.ATTN” ONLY EMPLOYED BEV QUERIES SELF-ATTENTION.

Fusion Method	Div.	Ped.	Bound.	mIoU
w/o SDMap	53.2	36.9	57.1	49.07
w/o SDMap, w/ Self.Attn.	57.7	42.0	60.6	53.43
Simply-concat	59.4	43.2	61.6	54.73
CNN-concat	60.2	45.5	63.1	56.27
Cross.Attn.	63.6	50.2	66.8	60.20

straightforward concatenation (termed “Simple-concat”) of the rasterized SDMap with BEV features led to a mIoU boost of about 5%. A better approach, where we exploit CNNs to encode and concatenate the rasterized SDMap, furthered this improvement to about 7%. Nonetheless, the straightforward concatenation techniques were hampered by spatial misalignment issues, preventing the full capitalization of the SDMap priors’ potential. Interestingly, leveraging self-attention solely for BEV queries also enhanced performance. Among all the approaches tested, our method anchored on cross-attention demonstrated the most substantial gains.

Ablation of BEV-SDPrior Cross-attention Layers. As the number of transformer layers increases, performance of our method improves, but it eventually reaches a point of saturation since the SDMap priors contain low-dimensional information, and excessively large network layers are susceptible to overfitting, as shown in Tab. VII.

TABLE VII

ABLATIONS ABOUT THE NUMBER OF BEV-SDPRIOR CROSS-ATTENTION LAYERS. DURING TRAINING, WE EVALUATED MEMORY USAGE WITH A BATCH SIZE OF 4, WHILE FOR INFERENCE, WE MEASURED FRAMES PER SECOND (FPS) WITH A BATCH SIZE OF 1.

Attention Layer	Div.	Ped.	Bound.	mIoU	Memory (GB)	FPS
1	62.6	48.4	65.6	58.87	19.03	19.60
2	63.6	50.2	66.8	60.20	20.20	18.56
4	60.6	44.9	63.2	56.23	23.24	18.45
6	58.7	42.4	61.8	54.30	OOM	-

The generalization capability of HDMap MAE. In order to verify the generalizability of our HDMap Prior refinement module, we pre-train on Argoverse2 and nuScenes datasets respectively, and fine-tune on nuScenes dataset and test the prediction results mIOU. The results are shown in the Tab. VIII, and it can be seen that the model pre-trained on

Argoverse2 is only 0.64% mIOU lower than the pre-trained model on nuScenes, which can prove that our refinement module indeed captures the HDMap priors information with generalization capability rather than overfitting to the dataset.

TABLE VIII

CROSS-DATASET EXPERIMENT OF HDMAP PRIORS. WE PRE-TRAINED THE HDMAP PRIOR MODULE ON ARGOVERSE2 AND NUSCENES DATASETS, RESPECTIVELY, AND TESTED IT ON NUSCENES VAL, USING A RANGE OF $120 \times 60m$ AND RGB+LIDAR INPUTS.

Pre-Train Dataset	Div.	Ped.	Bound.	mIoU \uparrow	LPIPS \downarrow
Argoverse v2	64.5	51.3	67.6	61.13 (+0.93)	0.7203 (8.49%)
Nuscense	65.3	52.0	68.0	61.77 (+1.57)	0.7124 (9.50%)

REFERENCES

- [1] Zhibin Bao, Sabir Hossain, Haoxiang Lang, and Xianke Lin. High-definition map generation technologies for autonomous driving. *ArXiv*, abs/2206.05400, 2022.
- [2] Holger Caesar, Varun Bankiti, Alex H Lang, Sourabh Vora, Venice Erin Liong, Qiang Xu, Anush Krishnan, Yu Pan, Giancarlo Baldan, and Oscar Beijbom. nuscenes: A multimodal dataset for autonomous driving. In *Proceedings of the IEEE/CVF conference on computer vision and pattern recognition*, pages 11621–11631, 2020.
- [3] Xiaoxue Chen, Hao Zhao, Guyue Zhou, and Ya-Qin Zhang. Pq-transformer: Jointly parsing 3d objects and layouts from point clouds. *IEEE Robotics and Automation Letters*, 7(2):2519–2526, 2022.
- [4] Wenjie Ding, Limeng Qiao, Xi Qiu, and Chi Zhang. Pivotnet: Vectorized pivot learning for end-to-end hd map construction, 2023.
- [5] Hao Dong, Xianjing Zhang, Xuan Jiang, Jun Zhang, Jintao Xu, Rui Ai, Weihao Gu, Huimin Lu, Juho Kannala, and Xieyuanli Chen. Superfusion: Multilevel lidar-camera fusion for long-range hd map generation and prediction. *arXiv preprint arXiv:2211.15656*, 2022.
- [6] Alexey Dosovitskiy, Lucas Beyer, Alexander Kolesnikov, Dirk Weissenborn, Xiaohua Zhai, Thomas Unterthiner, Mostafa Dehghani, Matthias Minderer, Georg Heigold, Sylvain Gelly, et al. An image is worth 16x16 words: Transformers for image recognition at scale. *arXiv preprint arXiv:2010.11929*, 2020.
- [7] Huan-ang Gao, Beiwen Tian, Pengfei Li, Xiaoxue Chen, Hao Zhao, Guyue Zhou, Yurong Chen, and Hongbin Zha. From semi-supervised to omni-supervised room layout estimation using point clouds. In *2023 IEEE International Conference on Robotics and Automation (ICRA)*, pages 2803–2810. IEEE, 2023.
- [8] Wenjie Gao, Jiawei Fu, Yanqing Shen, Haodong Jing, Shitao Chen, and Nanning Zheng. Complementing onboard sensors with satellite map: A new perspective for hd map construction, 2023.
- [9] Mordechai Haklay and Patrick Weber. Openstreetmap: User-generated street maps. *IEEE Pervasive computing*, 7(4):12–18, 2008.
- [10] Kaiming He, Xinlei Chen, Saining Xie, Yanghao Li, Piotr Dollár, and Ross Girshick. Masked autoencoders are scalable vision learners. In *Proceedings of the IEEE/CVF conference on computer vision and pattern recognition*, pages 16000–16009, 2022.
- [11] John Houston, Guido Zuidhof, Luca Bergamini, Yawei Ye, Long Chen, Ashesh Jain, Sammy Omari, Vladimir Iglovikov, and Peter Ondruska. One thousand and one hours: Self-driving motion prediction dataset. In *Conference on Robot Learning*, pages 409–418. PMLR, 2021.
- [12] Yihan Hu, Jiazhi Yang, Li Chen, Keyu Li, Chonghao Sima, Xizhou Zhu, Siqi Chai, Senyao Du, Tianwei Lin, Wenhai Wang, et al. Planning-oriented autonomous driving. In *Proceedings of the IEEE/CVF Conference on Computer Vision and Pattern Recognition*, pages 17853–17862, 2023.
- [13] Bu Jin, Xinyu Liu, Yupeng Zheng, Pengfei Li, Hao Zhao, Tong Zhang, Yuhang Zheng, Guyue Zhou, and Jingjing Liu. Adapt: Action-aware driving caption transformer. In *2023 IEEE International Conference on Robotics and Automation (ICRA)*, pages 7554–7561. IEEE, 2023.
- [14] Qi Li, Yue Wang, Yilun Wang, and Hang Zhao. Hdmapnet: An online hd map construction and evaluation framework. In *2022 International Conference on Robotics and Automation (ICRA)*, pages 4628–4634. IEEE, 2022.
- [15] Bencheng Liao, Shaoyu Chen, Bo Jiang, Tianheng Cheng, Qian Zhang, Wenyu Liu, Chang Huang, and Xinggang Wang. Lane graph as path: Continuity-preserving path-wise modeling for online lane graph construction. *arXiv preprint arXiv:2303.08815*, 2023.
- [16] Bencheng Liao, Shaoyu Chen, Xinggang Wang, Tianheng Cheng, Qian Zhang, Wenyu Liu, and Chang Huang. Maptr: Structured modeling and learning for online vectorized hd map construction. *arXiv preprint arXiv:2208.14437*, 2022.
- [17] Yicheng Liu, Yue Wang, Yilun Wang, and Hang Zhao. Vectormapnet: End-to-end vectorized hd map learning. *arXiv preprint arXiv:2206.08920*, 2022.
- [18] Zhijian Liu, Haotian Tang, Alexander Amini, Xinyu Yang, Huizi Mao, Daniela Rus, and Song Han. Bevfusion: Multi-task multi-sensor fusion with unified bird’s-eye view representation. *arXiv preprint arXiv:2205.13542*, 2022.
- [19] Bowen Pan, Jiankai Sun, Ho Yin Tiga Leung, Alex Andonian, and Bolei Zhou. Cross-view semantic segmentation for sensing surroundings. *IEEE Robotics and Automation Letters*, 5(3):4867–4873, 2020.
- [20] Jonah Philion and Sanja Fidler. Lift, splat, shoot: Encoding images from arbitrary camera rigs by implicitly unprojecting to 3d. In *Computer Vision—ECCV 2020: 16th European Conference, Glasgow, UK, August 23–28, 2020, Proceedings, Part XIV 16*, pages 194–210. Springer, 2020.
- [21] Avishkar Saha, Oscar Mendez, Chris Russell, and Richard Bowden. Translating images into maps. In *2022 International Conference on Robotics and Automation (ICRA)*, pages 9200–9206. IEEE, 2022.
- [22] Ashish Vaswani, Noam Shazeer, Niki Parmar, Jakob Uszkoreit, Llion Jones, Aidan N Gomez, Łukasz Kaiser, and Illia Polosukhin. Attention is all you need. *Advances in neural information processing systems*, 30, 2017.
- [23] Huijie Wang, Tianyu Li, Yang Li, Li Chen, Chonghao Sima, Zhenbo Liu, Bangjun Wang, Peijin Jia, Yuting Wang, Shengyin Jiang, et al. Openlane-v2: A topology reasoning benchmark for unified 3d hd mapping. *Advances in Neural Information Processing Systems*, 36, 2024.
- [24] Benjamin Wilson, William Qi, Tanmay Agarwal, John Lambert, Jagjeet Singh, Siddhesh Khandelwal, Bowen Pan, Ratnesh Kumar, Andrew Hartnett, Jhony Kaesemodel Pontes, Deva Ramanan, Peter Carr, and James Hays. Argoverse 2: Next generation datasets for self-driving perception and forecasting. In *Proceedings of the Neural Information Processing Systems Track on Datasets and Benchmarks (NeurIPS Datasets and Benchmarks 2021)*, 2021.
- [25] Zirui Wu, Tianyu Liu, Liyi Luo, Zhide Zhong, Jianteng Chen, Hongmin Xiao, Chao Hou, Haozhe Lou, Yuntao Chen, Runyi Yang, et al. Mars: An instance-aware, modular and realistic simulator for autonomous driving. In *CAAI International Conference on Artificial Intelligence*, pages 3–15. Springer, 2023.
- [26] Ziyang Xie, Ziqi Pang, and Yu-Xiong Wang. Mv-map: Offboard hd-map generation with multi-view consistency. *arXiv*, 2023.
- [27] Xuan Xiong, Yicheng Liu, Tianyuan Yuan, Yue Wang, Yilun Wang, and Hang Zhao. Neural map prior for autonomous driving. In *Proceedings of the IEEE/CVF Conference on Computer Vision and Pattern Recognition*, pages 17535–17544, 2023.
- [28] Tianyuan Yuan, Yicheng Liu, Yue Wang, Yilun Wang, and Hang Zhao. Streammapnet: Streaming mapping network for vectorized online hd map construction. *arXiv preprint arXiv:2308.12570*, 2023.
- [29] Gongjie Zhang, Jiahao Lin, Shuang Wu, Yilin Song, Zhipeng Luo, Yang Xue, Shijian Lu, and Zuoguan Wang. Online map vectorization for autonomous driving: A rasterization perspective. *arXiv preprint arXiv:2306.10502*, 2023.
- [30] Richard Zhang, Phillip Isola, Alexei A Efros, Eli Shechtman, and Oliver Wang. The unreasonable effectiveness of deep features as a perceptual metric. In *Proceedings of the IEEE conference on computer vision and pattern recognition*, pages 586–595, 2018.
- [31] Hao Zhao, Ming Lu, Anbang Yao, Yiwen Guo, Yurong Chen, and Li Zhang. Physics inspired optimization on semantic transfer features: An alternative method for room layout estimation. In *Proceedings of the IEEE conference on computer vision and pattern recognition*, pages 10–18, 2017.
- [32] Yupeng Zheng, Chengliang Zhong, Pengfei Li, Huan-ang Gao, Yuhang Zheng, Bu Jin, Ling Wang, Hao Zhao, Guyue Zhou, Qichao Zhang, et al. Steps: Joint self-supervised nighttime image enhancement and depth estimation. In *2023 IEEE International Conference on Robotics and Automation (ICRA)*, pages 4916–4923. IEEE, 2023.

A. Implementation Details

P-MapNet is trained with four NVIDIA GeForce RTX 3090 GPUs. We use the Adam optimizer and StepLR schedule for training with a learning rate of 5×10^{-4} . For fairness comparison, we adopt the EfficientNet-B0 pretrained on ImageNet as the perspective view image encoder and use a MLP to convert to the BEV features. To encode the point clouds for the LiDAR BEV features, we utilize the PointPillars framework, operating at an output dimension of 128. During the pretraining phase for the HDMap prior, we trained for 20 epochs for each range. Subsequently, we combined the *BEV Feature Fusion* with the *HDMap Prior Refinement* module and conducted an additional 10 epochs of training to obtain the final HDMap predictions.

B. Further Study on SDmap Prior

1) *Integrating SDMap Prior into end-to-end vectorized framework*: As demonstrated in Tab.IX, to confirm the universality of our SDMap prior, we integrated our SDMap Prior Module into MapTR (with only minor modifications), a state-of-the-art end-to-end framework, referred to as the MapTR-SDMap method. Our MapTR-SDMap method also led to a significant improvement in mean Average Precision (mAP).

The visualization results in Fig. 6 also show that MapTR-SDMap performs better under the most challenging $240 \times 60m$ ultra-long range of perception. It can also be seen that the segmentation-post-processing approach has stable results because it is sense-prediction, while the end-to-end vectorization approach still has some challenges such as significant predictive bias and challenges in keypoint selection. In conclusion, our proposed SDMap Prior fusion method demonstrates performance improvement in both the segmentation-postprocessing framework and the end-to-end framework.

TABLE IX

COMPARISONS WITH MAPTR ON nuSCENES *val* SET. WE CONDUCTED A COMPARISON BETWEEN MAPTR FUSED WITH THE SDMAP PRIOR METHOD (MAPTR-SDMAP) AND THE VANILLA MAPTR, USING ONLY SURROUND-VIEW CAMERAS AS INPUT AND WE USE PREDEFINED CD THRESHOLDS OF 0.5M, 1.0M AND 1.5M. OUR RESULTS DEMONSTRATED SUPERIOR PERFORMANCE, HIGHLIGHTING THE EFFECTIVENESS OF OUR SDMAP PRIOR FUSION METHOD.

Range	Method	Div.	Ped.	Bound.	mAP
$60 \times 30m$	MapTR	49.50	41.17	51.08	47.25
	MapTR-SDMap	50.92	43.71	53.49	49.37 (+2.21)
	P-MapNet	26.08	17.66	48.43	30.72
$120 \times 60m$	MapTR	26.00	18.89	15.73	20.20
	MapTR-SDMap	27.23	21.95	19.50	22.89 (+2.69)
	P-MapNet	19.50	24.72	42.48	28.90
$240 \times 60m$	MapTR	12.69	7.17	4.23	8.03
	MapTR-SDMap	22.74	16.34	10.53	16.53 (+8.50)
	P-MapNet	14.51	25.63	28.11	22.75

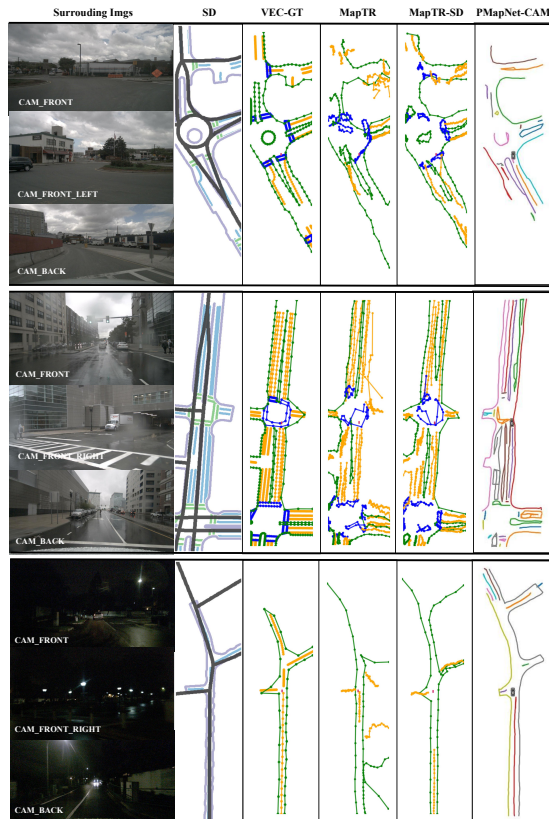


Fig. 6. The qualitative results of vectorized results on a perception range of $240m \times 60m$. We integrate the SDMap Prior Module into the MapTR (with only minor modifications), referred to as the MapTR-SD. PMapNet-CAM is our method with both SDMap prior and HDMap prior utilizing the post process.

2) *Inconsistencies between Ground Truth and SDMaps: Influence of Inconsistencies between Ground Truth and SDMaps*. Our SDMap priors are derived from OpenStreetMap (OSM). Nonetheless, due to discrepancies between labeled datasets and actual real-world scenarios, not all roads datasets are comprehensively annotated. This leads to incongruities between the SDMap and HDMap. Upon a closer examination of OSM, we noticed that there is a category in OSM called *service* road, which is for access roads leading to or located within an industrial estate, camp site, business park, car park, alleys, etc.

Incorporating *service* category roads can enrich the SDMap prior information with greater details. However, it also implies a potential increase in inconsistencies with dataset annotations. In light of this, we take ablation experiments to determine the advisability of incorporating *service* category roads.

As shown in Fig. 7, we select two cases to demonstrate the impact of inconsistencies between datasets map annotations and SDMaps. Specifically, in the Fig. 7(a), the inclusion of a *service* roads (an industrial estate) yields a positive outcome, where the SDMap aligns well with the ground truth dataset.

Nevertheless, in most cases, SDMaps with *service* roads

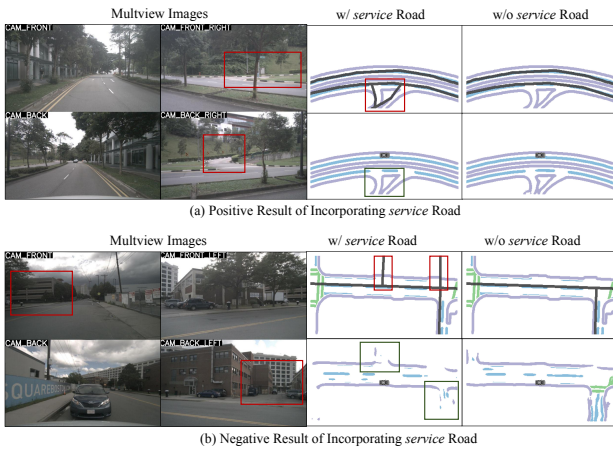


Fig. 7. The two scenarios underscore the effects of discrepancies between the ground truth and SDMaps. (b) shows that the network filters most of the *service* roads as noise since majority of them are incongruous with the ground truth, which affects the performance of trunk roads. SDMap prior exhibits commendable efficacy when *service* roads are not introduced. (a) demonstrates that when the distribution of the *service* road deviates from the norm, its performance is enhanced since the network refrains from filtering it out as noise.

are inconsistent with the ground truth of datasets, primarily due to the lack of detailed annotations for internal roads. Consequently, during the training process, the network learns the distribution of most service roads and filters them as noise. This inadvertently led to some primary roads being erroneously filtered out as noise. As depicted in Fig. 7(b), the service road (two alleys) highlighted in the red box is absent in the ground truth. The network perceives it as noise and consequently does not produce the corresponding road. However, it also neglects to generate a road for the primary route indicated in the ground truth, delineated within the green box, resulting in a significant discrepancy. Conversely, the network that excludes *service* roads avoids learning numerous erroneous SDMap distributions. This enables the network to more effectively assimilate SDMap information pertaining to main roads, even though many detailed SDMaps may be missing. The visualization in the right side of Fig. 7(b) demonstrates that the SDMap prior effectively guides the generation of HDMap. It even reconstructs the pedestrian crosswalks and lane at remote intersections, even though these reconstructions do not align with the actual ground truth.

TABLE X

QUANTITATIVE RESULTS ON DIFFERENT OSM CATEGORY.

INCORPORATING *service* ROAD INTRODUCE RICHER INFORMATION BUT ALSO INVOLVE INCONSISTENCY. IN TERMS OF SEGMENTATION mIoU RESULTS, THE ABSENCE OF *service* ROADS IN THE SDMAP PRIOR LEADS TO AN IMPROVEMENT OF APPROXIMATELY 2% IN PERFORMANCE.

With <i>service</i> road	Divider	Ped Crossing	Boundary	mIoU
w/ <i>service</i>	62.4	47.9	65.3	58.53
w/o <i>service</i>	63.6	50.2	66.8	60.20

In terms of quantitative metrics, as show in Tab. X, excluding *service* roads results in a 2% mIoU improvement.

The modest difference in these metrics suggests that the network can effectively filter out noise when introduced to numerous SDMaps that deviate from the ground truth. It further emphasizes the effectiveness of an SDMap focused on main roads in guiding the generation of the HDMap.

Visualization Analysis of the Inconsistencies between Ground Truth and SDMaps. As seen in Fig. 8, we select a case to show the negative result in the near side due to the inconsistencies. Obviously, the baseline shows that when SDMap prior information is not integrated, both the left and right forks at the near side can be predicted, but the far side cannot be predicted clearly due to weather reasons and visual distance.

When leveraging the SDMap prior to bolster HDMap generation, the predictions for the near side forks roads deteriorate due to the SDMap’s exclusive focus on trunk roads. Furthermore, incorporating the HDMap prior alleviates artifacts and bridges the gaps, but this inadvertently diminishes prediction performance on the near side fork roads, as shown in Fig. 8(a).

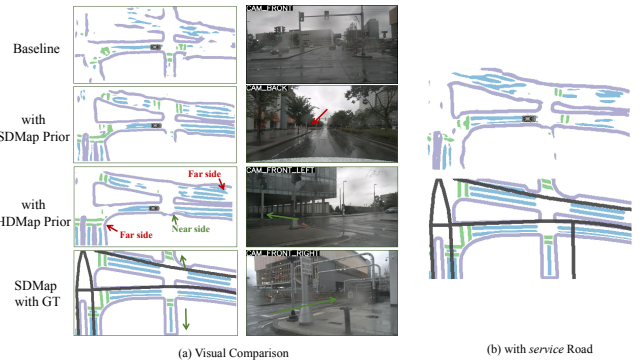


Fig. 8. **The negative results in the near side fork roads.** (a) demonstrates that the baseline exhibits proficient performance in predicting near side forks. Yet, due to the SDMap’s exclusive focus on main roads, the prediction accuracy for near side forks diminishes upon integrating both the SDMap and HDMap prior information. (b) shows that even if *service* road information is added, the network will filter out this SDMap as noise.

However, we also validate the case using the model with *service* roads as in Fig. 8(b). The network perceives the *service* SDMap of the fork road (to the industrial park) as noise and filters it out, as mentioned in the previous part. The other left side fork road is not contained in the *service*. Consequently, it performs suboptimal as well since the SDMaps is not detailed enough and the discrepancies between SDMaps and dataset’s ground truth.

In summary, we introduce SDMap priors information and undertaken a comprehensive analysis of several intriguing cases. Our intent is to offer insights that may inspire future researchers to further the utilization of SDMap priors in HDMap generation.

3) *Ablation of BEV Feature Downsampling Factor:* Different downsampling factor d impact the size of feature map \mathcal{B}_{small} in the fusion module. Larger feature maps convey more information but can result in higher GPU memory usage and slower inference speed. As shown in Tab. XI, to

strike a balance between speed and accuracy, we opt for a size of 50×25 .

TABLE XI

ABLATIONS ABOUT DOWNSAMPLING FACTOR. WE CONDUCTED A COMPARISON OF mIOU RESULTS FOR FEATURE SIZES AT A RANGE OF $120 \times 60m$ WITH DIFFERENT DOWN-SAMPLING MULTIPLES. THE TERM “OOM” REPRESENTS THE GPU MEMORY IS EXHAUSTED. DURING TRAINING, WE EVALUATED MEMORY USAGE WITH A BATCH SIZE OF 4, WHILE FOR INFERENCE, WE MEASURED FRAMES PER SECOND (FPS) WITH A BATCH SIZE OF 1.

Factor	Feature Map Size	Div.	Ped.	Bound.	mIoU	Memory(GB)	FPS
$d = 2$	100×50	-	-	-	-	OOM	-
$d = 4$	50×25	63.6	50.2	66.8	60.20	20.2	18.56
$d = 8$	25×12	60.7	45.0	63.3	56.33	18.3	19.60

TABLE XII

ABLATIONS ABOUT MASK PROPORTION. WE USE DIFFERENT RANDOM MASK RATIOS FOR PRE-TRAINING, WITH HIGHER MASK RATIOS BEING HARDER FOR THE RECONSTRUCTION.

Mask Proportion	Divider	Ped Crossing	Boundary	mIoU
25%	64.8	51.4	67.6	61.27
50%	65.3	52.0	68.0	61.77
75%	64.7	52.1	67.7	61.50

C. Further Study on HDmap Prior

1) *Mask proportion Experiment:* As show in Tab. XII, we test the effect of using different mask ratios for pre-training on the refinement results, too high a mask ratio will lead to the lack of valid information and the actual refinement process of the input difference is large, too low a mask ratio can not force the network to capture the HDMap priors, we choose the optimal 50% as the ratio of pre-training of our method.

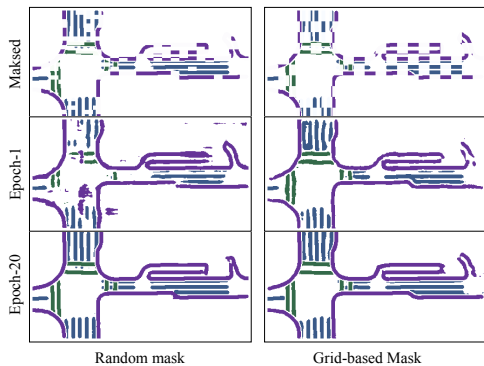


Fig. 9. **Different mask strategies.** “Maksd” refers to the pre-training inputs after applying various masking strategies, and “Epoch-1” and “Epoch-20” denote the reconstruction results at the first and twentieth epochs of the pre-training process, respectively.

2) *Ablation of Mask Strategy:* The grid-based strategy uses a patch size of 20×20 pixels and keeps one of every two patches. And the random-mask strategy selects one of the patch sizes from 20×20 , 20×40 , 25×50 , or 40×80 with a 50% probability for masking. The visualization results

are presented in Figure 9. With pre-training, the refinement module effectively learns the HDMap priors. As depicted in Tab.XIII, our approach employing the random sampling strategy yielded the most favorable results.

TABLE XIII

ABLATIONS ABOUT MASK STRATEGY. “w/o PRETRAIN” SIGNIFIES THAT WE DO NOT PRE-TRAIN THE HDMAP PRIOR REFINEMENT MODULE. INTERESTINGLY, OUR RANDOM-MASK METHOD YIELDS SUPERIOR RESULTS IN THIS CONTEXT.

Mask Strategy	Divider	Ped Crossing	Boundary	mIoU
w/o Pre-train	64.1	51.4	67.4	60.97
Grid-based	65.1	52.3	67.8	61.73
Random-mask	65.3	52.0	68.0	61.77

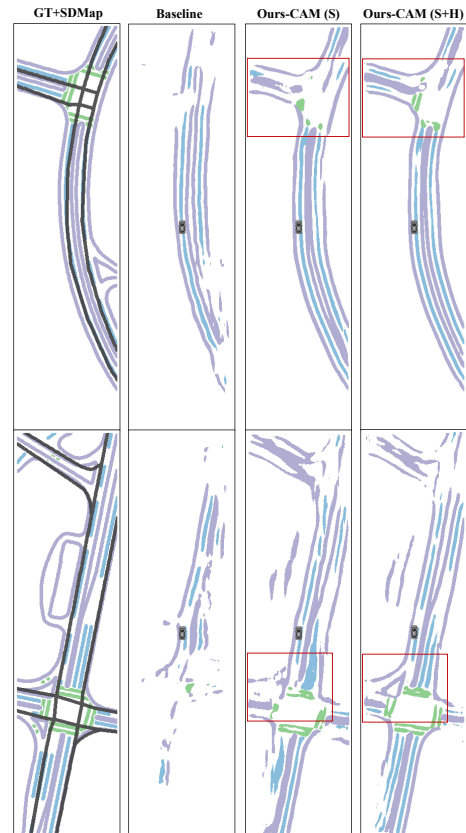


Fig. 10. **The qualitative results of only camera method on a perception range of $240m \times 60m$.** The SDMap Prior Module improves the prediction results by fusing road structure priors. While HDMap Prior Module makes it closer to the distribution of HDMap to a certain extent, making it look more realistic.

D. QUALITATIVE VISUALIZATION

1) *Segmentation Qualitative Results:* As depicted in the Fig.10 and Fig. 6, we provide additional perceptual results under diverse weather conditions, and our method exhibits superior performance.

2) *SD Map Data Visualization:* We supplemented the SD Map data on both the and datasets, the specific details are outlined in Tab. XIV. The visualization of SD map data and

HD Map data facilitated by the dataset, is presented in Fig. 11 and Fig. 12.

TABLE XIV

SDMAP DATA DETAILS. IN ORDER TO GENERATE THE SDMAP DATA, WE EXTRACT THE *road*, *road link* AND *special road* DATA FROM THE *highway section* OF OSM DATA AND PERFORM COORDINATE ALIGNMENT AND DATA FILTERING.

Dataset	Sub-Map	Lane Numbers	Total Length(km)
NuScenes	Singapore-OneNorth	576	23.4
	Singapore-HollandVillage	359	16.9
	Singapore-Queenstown	393	17.9
	Boston-Seaport	342	32.1
Argoverse2	Austin	193	46.5
	Detroit	853	160.6
	Miami	1226	178.2
	Palo Alto	315	33.4

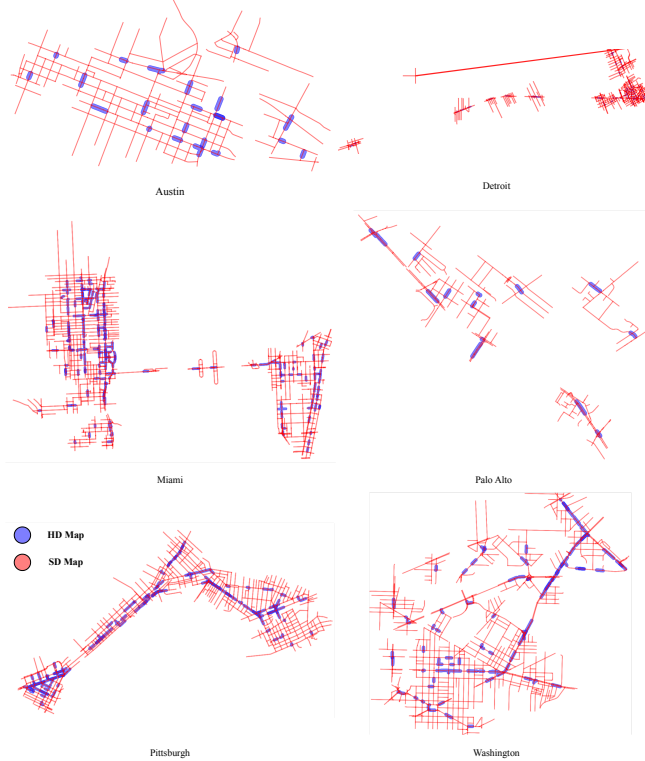


Fig. 11. The visualizations of SD Map data and HD Map data on the Argoverse2 dataset.



Fig. 12. The visualizations of SD Map data and HD Map data on the nuScenes dataset.